

Solubility of water in bridgmanite

Wenhua Lu^{1,2,3}  · Yuan Li^{1,2}

Received: 31 July 2023 / Revised: 2 September 2023 / Accepted: 24 September 2023 / Published online: 4 October 2023
© The Author(s), under exclusive licence to Science Press and Institute of Geochemistry, CAS and Springer-Verlag GmbH Germany, part of Springer Nature 2023

Abstract Water in Earth's mantle plays a critical role in both geodynamic and surficial habitability. Water in the upper mantle and transition zone is widely discussed, but less is known about the water in the lower mantle despite it constituting over half of Earth's mass. Understanding the water storage in Earth's lower mantle relies on comprehending the water solubility of bridgmanite, which is the most abundant mineral both in the lower mantle and throughout Earth. Nevertheless, due to limited access to the lower mantle, our understanding of water in bridgmanite mainly comes from laboratory experiments and theoretical calculations, and a huge controversy still exists. In this paper, we provide a review of the commonly employed research methods and current findings concerning the solubility of water in bridgmanite. Potential factors, such as pressure, temperature, compositions, etc., that influence the water solubility of bridgmanite will be discussed, along with insights into future research directions.

Keywords Water solubility · Bridgmanite · Lower mantle · Habitability

✉ Wenhua Lu
wenhualu@gig.ac.cn

Yuan Li
Yuan.Li@gig.ac.cn

¹ State Key Laboratory of Isotope Geochemistry, Guangzhou Institute of Geochemistry, Chinese Academy of Sciences, Guangzhou 510640, China

² CAS Center for Excellence in Deep Earth Science, Guangzhou 510640, China

³ College of Earth and Planetary Sciences, University of Chinese Academy of Sciences, Beijing 100049, China

1 Introduction

Water (referring to hydrogen-bearing ions or molecules) is an essential component of a habitable Earth, which is not only distributed on the surface but also exists in Earth's interior (Peslier et al. 2017; Li et al. 2020; Ohtani 2021). Water in the Earth's interior could significantly reduce the viscosity and melting temperature of rocks (Gaetani and Grove 1998; Genova et al. 2023), thereby accelerating the circulation of materials within the Earth's interior. Understanding the abundance and distribution of water in the mantle is fundamental to unravel its differentiation and evolutionary processes.

Based on extensive geochemical, geophysical observations, and high-temperature and high-pressure (HPHT) experimental studies, the water content of the upper mantle is well constrained, with an estimated value of $\sim 200 \text{ }\mu\text{g/g}$ (Hirschmann 2006; Peslier et al. 2017), corresponding to ~ 0.1 ocean mass water (one ocean mass = $1.4 \times 10^{21} \text{ kg}$). The water content of the mantle transition zone remains under debate, with estimated total water budgets ranging from ~ 0.1 to 5.8 ocean masses (Karato 2011; Fei et al. 2017; Zhang et al. 2022). But the mantle transition zone appears to contain more water than the upper mantle because water solubilities of the major minerals in the mantle transition zone (e.g., wadsleyite and ringwoodite) are significantly greater than those in the upper mantle (Keppler and Bolfan-Casanova 2006; Inoue et al. 2010). The water content in the lower mantle currently is highly uncertain, with only sporadic studies suggesting that there are some hydrous regions in the shallow lower mantle (Liu et al. 2016; Gu et al. 2022). For example, Gu et al. (2022) found hydrous peridotitic fragments in the inclusions of ultra-deep diamonds possibly from the topmost lower

mantle. However, the representativeness of these samples and the water content in the deeper lower mantle remain unknown.

Ocean island basalts (OIB) are usually used to probe the geochemistry of the lower mantle due to their deep sources that possibly extend to the core-mantle boundary as shown by the seismic observations (French and Romanowicz 2015). Overall, OIB generally has higher water content compared to mid-ocean ridge basalts (MORB) derived from the depleted mantle (Moore 1970; Hallis et al. 2015; Liu et al. 2017a). Hirschmann and Dasgupta (2009) estimated that the water content in the mantle sources of OIB is ~0.2–1.6 times higher than that of MORB based on H/C ratios. However, whether the source of OIB can represent the entire lower mantle remains unclear, because some of the water in OIB may be contributed by the recycled lithosphere (Dixon et al. 2002). Marty (2012) proposed that the whole mantle is required to contain about 10 ± 5 ocean masses of water to match the cosmochemical observations of noble gas in the bulk silicate Earth. However, the upper mantle and mantle transition zone could only account for ~7 ocean masses of water at maximum if they are both water-saturated (Karato et al. 2020). It means that the lower mantle has to contain at least ~3 ocean masses of water to satisfy the estimate from Marty (2012). The maximal water capacity of the lower mantle hence becomes a key parameter for judging the validity of the estimates of water in the mantle. Additionally, the water capacity of the mantle also plays a critical role in regulating its dehydration processes and the water cycle within Earth (Bercovici and Karato 2003).

Bridgmanite, the $(\text{Mg}, \text{Fe})\text{SiO}_3$ perovskite in an orthorhombic structure (Tschauner et al. 2014), is the most abundant mineral in the lower mantle. Bridgmanite comprises approximately 75–80 % volume of the lower mantle when in pyrolite or harzburgite composition and around 35 % when in subducted slab composition [see Irfune and Tsuchiya (2015) and references therein]; hence, its water solubility is of first-order importance to determine the water capacity of the lower mantle. Extensive attempts have been made to investigate the water solubility of bridgmanite using various approaches, but a consensus has not yet been reached. This review paper will first introduce the methods for studying the solubility of water in bridgmanite then summarize the results we now have. Factors that may influence the solubility of water in bridgmanite will be discussed subsequently with some perspectives proposed for future studies.

2 Methods for studying solubility of water in bridgmanite

The HTHP experiment and first-principles simulation are two primary methods for studying the water solubility of bridgmanite because natural samples derived from the lower mantle are rare. Bridgmanite stabilization requires pressure over 23 GPa at mantle adiabatic (Ito and Weidner 1986), which makes it challenging to be studied in a laboratory.

When employing the HTHP experimental method, two steps are necessary: (1) synthesizing clear bridgmanite samples under extreme pressure-temperature (P-T) conditions in a water-saturated system; and (2) accurately determining the water content of the obtained bridgmanite through HTHP experiments. Multi-anvil apparatus and laser-heated diamond anvil cell (DAC) are generally employed to generate the P-T conditions of the lower mantle. However, quantifying the water content of sample recovered from HPHT experiments is challenging because (1) the synthesized bridgmanite are often accompanied by water-rich melt, making it difficult to be separated cleanly and (2) the size of synthesized bridgmanite is usually small. For example, bridgmanite crystals recovered from multi-anvil experiment typically do not exceed 400 μm and is often only tens of micrometers; the DAC samples, on the other hand, are usually smaller than 5 μm .

Fourier transform infrared absorption spectroscopy (FTIR) and secondary ion mass spectrometry (SIMS) are two techniques that are widely used to measure the water content of a sample. They both have high sensitivity with detection limits generally less than 10 $\mu\text{g/g}$ (Rossman 2006). FTIR has the advantage of not damaging the sample and can also determine the bonding types of hydrogen simultaneously. However, the sample requires double-sided polishing and the accuracy of the measurement largely depends on the choice of calibration coefficients (Paterson 1982; Libowitzky and Rossman 1997; Koga et al. 2003). SIMS determines the total water content of a sample with detected limits as low as 1 $\mu\text{g/g}$ (Newcombe et al. 2023). Furthermore, the nanoscale secondary ion mass spectrometry (NanoSIMS) could have spatial resolution reaching to nanometer level (Saal et al. 2008) and is a powerful technique available for quantitatively analyzing water content in small ultra-high pressure samples (Yang et al. 2023). However, both SIMS and NanoSIMS have several disadvantages. Firstly, they cause irreversible damage to the sample, preventing repeat measurements.

Secondly, they are unable to exclude the water in the inclusions (fluid or melt), hydrous phases, and/or other impurities that formed within the experimentally-produced bridgmanite samples. Lastly, the matrix effects need to be addressed. In recent years, atom probe tomography (APT) has rapidly emerged as a potential technique for quantitatively analyzing the composition of small samples. It can not only accurately analyze the water content but also provide information on the spatial distribution of water in the sample (Gault et al. 2021). However, the sample pre-treatment for APT analysis is complicated. At present, no examples of its application in bridgmanite water solubility studies have been seen (Reddy et al. 2020).

The first-principles simulation is readily to simulate the P–T conditions of bridgmanite stability. The essence of this method is to solve the Schrödinger equation, which determines the position of the atomic nucleus by considering the fundamental laws governing the interaction between atomic nuclei and electrons (Stixrude 2001). Free energy is calculated iteratively using a path integral and subsequently converted into thermodynamic parameters based on thermodynamic derivation. However, it is necessary to possess an accurate equation of state of the material before conducting the simulation to obtain an accurate P–T. Additionally, simulation of multiple atoms entails significant time and computational resources, thereby a very simple mineral composition under an ideal case is usually assumed. However, this assumption may not be true since the natural system is highly non-ideal. Various factors such as composition, as well as variables like P and T, can potentially affect the solubility of water in bridgmanite.

3 Results of water solubility of bridgmanite

Table 1 summarizes the solubility of water in bridgmanite that has been reported so far, most of which were obtained through HTHP experiments with some from calculations. There is still no consensus on the water solubility of bridgmanite so far.

3.1 Water solubility in bridgmanite constrained by multi-anvil experiments

The multi-anvil apparatus has been widely used to synthesize water-saturated bridgmanite at conditions of the lower mantle since the 1990s, yet a unified understanding of water solubility of bridgmanite has not been achieved (Fig. 1). Meade et al. (1994) first reported the water content of synthetic bridgmanite recovered from 27 GPa and 2103 K. They found bands at 3483 and 3423 cm⁻¹ using synchrotron radiation FTIR and estimated the water

content of the bridgmanite at ~ 105 µg/g (Meade et al. 1994), suggesting that the lower mantle can accommodate a large amount of water in bridgmanite. However, Bolfan-Casanova et al. (2000) obtained different results in their experiments, where bridgmanites synthesized at 24 GPa, 1873 K, and water-saturated conditions did not show any hydrogen-related bands in the IR spectra, indicating the water content should below the detection limit (< 1 µg/g). Bolfan-Casanova et al. (2000) speculated that the experiment of Meade et al. (1994) might not reach equilibrium because the experiment only lasted for 8 mins (Ito and Weidner 1986).

Bridgmanite in the lower mantle is unlikely to be pure MgSiO₃ and should be Al- and Fe-bearing (Ito et al. 2004). To investigate the effect of Al and Fe, Murakami et al. (2002) synthesized Al- and Fe-bearing bridgmanites at 25.5 GPa and 1873–1973 K and found bands at ~ 3400 cm⁻¹ in the IR spectra of the recovered bridgmanites. Combined with SIMS analysis, they showed that the water solubility of bridgmanite could be up to 2400 µg/g (Murakami et al. 2002), which is significantly higher than the results of Bolfan-Casanova et al. (2000). Subsequently, Litasov et al. (2003) synthesized bridgmanites with various Al and Fe contents at 25 GPa, 1273–1873 K, and water-saturated conditions. IR spectra of recovered bridgmanite also show bands at ~ 3400–3500 cm⁻¹ and the water solubilities were determined in the range of 47–1780 µg/g (Litasov et al. 2003). To address this contradiction, Bolfan-Casanova et al. (2003) synthesized Al- and Fe-bearing bridgmanite at 24 GPa and 1673 K in a water-saturated system and also observed bands at 3350, 3410, and 3640 cm⁻¹ in the IR spectra of bridgmanite. However, Raman spectra of the sample show peaks that can be referred to as superhydrous phase B, indicating that these IR bands are likely caused by water-rich inclusions between or in the bridgmanite grains rather than in its crystal structure (Bolfan-Casanova et al. 2003).

Inoue et al. (2010) conducted experiments at 23 GPa and 1873 K using Fe-bearing initial materials with water content of 15.8 wt% to determine the partition coefficient of water between the transition zone and lower mantle minerals. Fe-bearing bridgmanites coexisting ringwoodite and hydrous silicate melt were obtained with water contents measured up to 700 µg/g using SIMS (Inoue et al. 2010). However, they did not provide a detailed analysis to confirm whether the bridgmanite contains water-rich inclusions. To address the “water-rich inclusions” problem, Fu et al. (2019) used transmission electron microscopy (TEM) to check the purity of the bridgmanite synthesized at 24 GPa and 2073 K using Al- and Fe-bearing initial materials. Water contents of the bridgmanites were determined up to ~ 1000 µg/g using both FTIR and SIMS, which is much

Table 1 Compilation of water solubility of bridgmanite

Reference	<i>P</i> (GPa)	<i>T</i> (K)	Run no.	Starting materials	^a H ₂ O solubility in Brg (μg/g)
Experimental results					
Meade et al. (1994)	27	2103		MgSiO ₃ + 50 wt% H ₂ O	105(25)
Murakami et al. (2002)	25.5	1873	C157	75.5 wt% KLB-1 + 11.5 wt% CaSiO ₃ + 13.5 wt% H ₂ O	2300(100)
	25.5	1893	C165	64.0 wt% KLB-1 + 25.0 wt% CaSiO ₃ + 11.0 wt% H ₂ O	1900(100)
	25.5	1923	C183	42.5 wt% KLB-1 + 38.9 wt% CaSiO ₃ + 11.1 wt% FeO + 7.5 wt% H ₂ O	2400(100)
Bolfan-Casanova et al. (2003)	24	1673	H1311	MgSiO ₃ + 10 wt% Al ₂ O ₃ + 5 wt% H ₂ O	1(1)
	24	1673	H1302	Glass + brucite	2(5)
Litasov et al. (2003)	25	1573	K-202	MgSiO ₃ + 10 wt% H ₂ O	300(100)
	25	1673	K-200	MgSiO ₃ + 10 wt% Al ₂ O ₃ + 10 wt% H ₂ O	101(19)
	25	1473	K-165	MORB-related Al-bearing bridgmanite (FeO free) + 5 wt% H ₂ O	1400(400)
	26	1473	K-164	MORB-related Al-bearing bridgmanite (FeO free) + 10 wt% H ₂ O	1400(400)
	26	1273	K-160	MORB-related (Al, Fe)-bearing bridgmanite + 5 wt% H ₂ O	110(21)
	26	1473	K-161		600(200)
	25	1573	K-205	MORB-related bridgmanite (TiO ₂ free) + 8 wt% H ₂ O	47(12)
	25	1673	K-208	Peridotite-related bridgmanite + 10 wt% H ₂ O	1780(175)
	25	1873	K-209		1460(130)
Inoue et al. (2010)	23.1	1873	E1730	(Mg _{0.8} Fe _{0.2}) ₂ SiO ₄ + 15.8 wt% H ₂ O	300
	23.2	1873	E1695		700(300)
Panero et al. (2015)	33	1600	710Ha	Enstatite with Mg/(Mg + Fe) = 0.87, < 0.1 wt% Al ₂ O ₃ + 2065 μg/g H ₂ O	10
	42	1900	0608Ha		220
Fu et al. (2019)	24	2073	5K2667-P1	21.6 wt% Mg(OH) ₃ + 58.8 wt% MgSiO ₃ + 11.8 wt% Al ₂ O ₃ + 7.8 wt% FeO	1005(68)
	24	2073	5K2667-P2		1031(81)
Liu et al. (2021)	24	1900	S7119	En90Cor10 + 8.8 wt% H ₂ O oxide mix	15(5)
	26	1900	IRIS669	En90Brm10 glass + 6 wt% H ₂ O	31(11)
	26	1900	S7158	En90FA10 glass + 10 wt% H ₂ O	12(2)
Ishii et al. (2022)	28	1273–1873		(70–90) wt% MgSiO ₃ + (10–30) wt% Al(OH) ₃ [(7.5–22.5) wt% H ₂ O]	< 1
Yang et al. (2023)	33	3690		Modified pyrolite composition	> 1099(14)
Computational results					
Hernández et al. (2013) ^b	24	1500 – 2000		MgSiO ₃ + Mg ₂ SiO ₄	770–1000
Panero et al. (2015)	25–125	2000–3000		MgSiO ₃ – MgO + δAlOOH	31–37
Townsend et al. (2015, 2016) ^b	110–135	2000–4000		H-bearing MgSiO ₃	1250– 6667
				H- and Al-bearing MgSiO ₃	50,000 –10,000

^aFor samples that both FTIR and SIMS measurements are available, the larger values are taken as the solubility and used in Fig. 1. ^b In these studies, the water solubilities are inferred from the water partition coefficient among solid minerals, see the main text for detailed discussions

higher than those reported by Bolfan-Casanova et al. (2000, 2003).

To verify the results of Fu et al. (2019), Liu et al. (2021) conducted similar experiments using Al- and Fe-bearing initial materials with water content of 6 – 10 wt% at

24–26 GPa and 1900 K. To minimize the effect of water-rich inclusions, the experimental durations were prolonged to 30 h. They obtained pure and transparent bridgmanites in the absence of bands at 3350–3690 cm⁻¹ in IR spectra, and hence they suggested that water solubility of

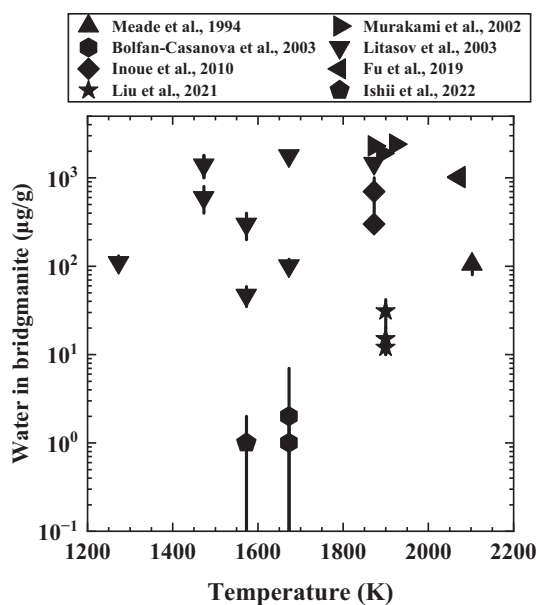


Fig. 1 Water solubility in bridgmanite obtained from multi-anvil experiments

bridgmanite should be $< 30 \mu\text{g/g}$ (Liu et al. 2021). These results were later confirmed by Ishii et al. (2022), who synthesized Al-rich bridgmanite at 25–28 GPa and 1273–1373 K with the existence of hydrous minerals and found that the water content of synthesized bridgmanite was lower than the detection limit ($\sim 1 \mu\text{g/g}$) of FTIR, supporting that bridgmanite is dry at the top lower mantle.

3.2 Results from laser-heated diamond anvil cell experiments

Limited researches have been conducted on studying water solubility of bridgmanite using laser-heated DAC compared to those using multi-anvil. The main obstacle comes from quantitative analysis of water content in tiny ($< 5 \mu\text{m}$) recovered samples. And up to now, a consistent understanding has yet to be achieved.

Schmandt et al. (2014) conducted pioneering experiments, where the synthetic hydrous ringwoodites were used as the starting materials and laser-heated to 1873 K under 30 GPa. The researchers subsequently analyzed the products using synchrotron radiation FTIR and observed bands at 3400 and 3680 cm^{-1} . However, the presence of hydrous melt and brucite around the bridgmanite indicates that these bands may represent water in the melt or brucite [Mg(OH)_2] rather than water in bridgmanite (Schmandt et al. 2014). In a subsequent study, Panero et al. (2015) employed enstatites with different water contents (35 and 2065 $\mu\text{g/g}$) as starting materials and laser-heated the samples to 1600–2000 K at pressures of 33–60 GPa; using synchrotron radiation FTIR, they identified four stretching

bands (3576, 3378, 3274, and 3078 cm^{-1}) in the IR spectra of the recovered samples that were cooled below 100 K. Although the total water content estimated from these bands could reach 220 $\mu\text{g/g}$, the actual water content within the bridgmanite should not exceed 10 $\mu\text{g/g}$ if considering the melt dispersed within the mineral interstices (Panero et al. 2015).

In the two aforementioned studies, there was a failure to completely separate the silicate melt and bridgmanite in the run products. Consequently, the exact water content of the bridgmanite could not be accurately quantified. Yang et al. (2023) melted a hydrous silicate glass at 33 GPa via laser-heated DAC experiments, where the bridgmanites grown at a liquidus temperature of 3690 K were completely separated with the silicate melt. NanoSIMS analysis demonstrated a water content of $\sim 1100 \mu\text{g/g}$ in the bridgmanite when in equilibrium with the silicate melt containing ~ 4.4 wt% water (Yang et al. 2023). It means that under these experimental conditions, water solubility of bridgmanite must be larger than 1100 $\mu\text{g/g}$, contradicting that bridgmanite is dry.

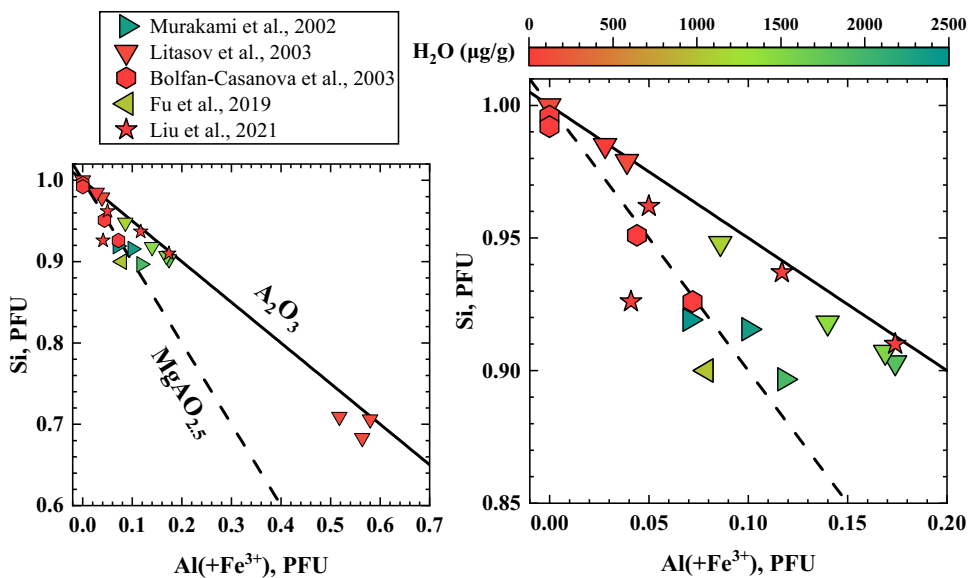
3.3 Results from first-principles simulations

It is challenging to investigate the solubility of water in bridgmanite using first-principles simulations due to the accuracy of simulating melts or fluids. Up to now, the first-principles simulations only yield accurate results in water partitioning among solid phases, from which one can estimate the water solubility of bridgmanite by knowing the water solubility of another phase.

Simulations from Hernández et al. (2013) suggested that the partition coefficients of water between ringwoodite and bridgmanite are 10–13, which aligns with the experimental results of Inoue et al. (2010). The solubility of water in bridgmanite hence could be estimated to be up to 1000 $\mu\text{g/g}$ (Hernández et al. 2013) given ringwoodite's water solubility of 1 wt% (Fei and Katsura 2020). However, Panero et al. (2015) found that water content of bridgmanite in equilibrium with stishovite should not exceed 43 $\mu\text{g/g}$ according to the calculated partition coefficient of water between bridgmanite and stishovite in a $\text{MgSiO}_3\text{-MgO} + \delta\text{AlOOH}$ binary system.

Bridgmanite could change its structure from perovskite to post-perovskite in the lowermost mantle conditions (e.g., Murakami et al. 2004; Oganov and Ono 2004). Townsend et al. (2015) conducted calculations and found that the post-perovskite structure can accommodate 1–2 wt% water. In their subsequent work, the partition coefficient of water between bridgmanite and post-perovskite is calculated to be 5 (Townsend et al. 2016), which means that the maximum water content in bridgmanite in equilibrium with water-saturated post-perovskite can reach 5–10 wt%.

Fig. 2 Substitution mechanism of trivalent cation into bridgmanite and its relationship with H_2O solubility. PFU: per formula unit

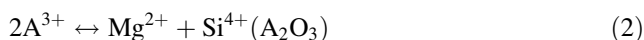


However, if the system is Al-bearing, the partition coefficient of water between bridgmanite and post-perovskite would decrease to 1/3–1/8 (Townsend et al. 2016), yielding the maximum water content in Al-bearing bridgmanite of approximately 0.13–0.67 wt%. However, it is worth noting that first-principles simulations typically assume a simplistic system, whereas the incorporation of water in real mantle minerals exhibits substantial non-ideality. This discrepancy may explain why the simulation results exhibit higher values compared to the experimental findings.

4 Discussion and future perspective

4.1 Potential substitution mechanism of H in bridgmanite

The chemical formula of pure bridgmanite is $MgSiO_3$, which belongs to nominally anhydrous minerals. However, under the conditions of the lower mantle, some cations can dissolve into bridgmanite and may affect its water solubility. For example, Navrotsky and colleagues (1999; 2003) proposed that trivalent cations (A^{3+} , $A = Al, Fe$) can dissolve into bridgmanite by substituting Si forming $MgAO_{2.5}$ or substituting Mg and Si forming A_2O_3 (Fig. 2), which could be expressed as:



where the Ov in Eq. (1) is the generated oxygen vacancy. If forming $MgAO_{2.5}$, the oxygen vacancies are potentially to be occupied by OH^- in a water-rich environment, thus introducing H into bridgmanite; whereas if forming A_2O_3 ,

the amount of H incorporated into bridgmanite would be limited. The first substitution mechanism was adopted to explain the high solubility of water in Al- and Fe-bearing bridgmanite (Murakami et al. 2002; Litasov et al. 2003; Fu et al. 2019). However, experiments by Bolfan-Casanova et al. (2003) and Liu et al. (2021) do not support this explanation. As shown in Fig. 2, bridgmanite with composition falling on the $MgAO_{2.5}$ substitution line does not always have high water solubility. Townsend et al. (2016) conducted first-principles simulations and found that H^+ together with Al^{3+} could directly substitute Si^{4+} in bridgmanite:



In this way, the Al-bearing bridgmanite could contain water up to 1000 µg/g (Townsend et al. 2015, 2016). However, there is a lack of experimental evidence to substantiate this substitution mechanism. Additionally, the Mg^{2+} in bridgmanite could also be substituted by divalent Fe or Ca ions (Boujibar et al. 2016; Liu et al. 2020; Ko et al. 2022). Based on the analysis of the Laplacian of the electron density distribution function, Ross et al. (2003) found that the Mg site is the only potential site for H entering bridgmanite via:



This substitution mechanism has been confirmed by a study using the first-principles simulation (Townsend et al. 2016), although the experimental evidence remains lacking. One important implication is that H could directly enter the lattice of bridgmanite in this way. If this is the case, one can expect that substantial water would be incorporated in bridgmanite; yet experimental verification is urgently required.

4.2 Factors that may control water solubility in bridgmanite

Bridgmanite is stable at depths from 660 km to the bottom of the mantle (Murakami et al. 2004), where the P–T conditions could change from ~23 GPa and 2000 K to ~125 GPa and 4000 K (Boehler 2000; Fiquet et al. 2010) with oxygen fugacity varying by several orders of magnitude (Frost and McCammon 2008). Moreover, bridgmanite could also transfer to other phases (such as corundum, etc.) within the mid-lower mantle regions of the subducted slabs (Liu et al. 2017b, 2020). Therefore, various factors, including P–T and oxygen fugacity, could potentially influence the solubility of water in bridgmanite.

The P–T conditions of related multi-anvil experiments are limited to 2103 K and 27 GPa, which are far from covering the P–T conditions of the whole lower mantle. Although laser-heated DAC experiments can achieve more extreme P–T conditions, quantitatively analyzing the water content of tiny recovered samples is a significant challenge. Yang et al. (2023) established a workable protocol to measure the water content of DAC sample using Nano-SIMS and found that the partition coefficient of water between bridgmanite and melt could be as high as ~0.025 at 33 GPa and 3690 K. Assuming that the partition coefficient of water is constant even when the activity of water in the melt equals to 1, then the maximal water content in bridgmanite would reach ~2.5 wt%, which is dramatically higher than all the values obtained from multi-anvil experiments. Further experiments at more extreme P–T conditions are urgently needed.

The incorporation mechanism of H into the bridgmanite could be influenced by the oxygen fugacity, which not only alters the $\text{Fe}^{3+}/\sum\text{Fe}$ of bridgmanite (Boujibar et al. 2016; Kuwahara and Nakada 2023) but also controls the H species in the hydrous melt or fluid that in equilibrium with the bridgmanite. For example, some low-pressure (<3 GPa) experiments have shown that at oxygen fugacity of 2 orders magnitude below the iron-wüstite buffer, more than half of the H in a silicate melt containing 3000 µg/g water will exist in the form of H_2 molecules (Hirschmann et al. 2012). As a result, some nominally anhydrous minerals (olivine or pyroxene) could incorporate H in the form of H_2 (Yang et al. 2016). And if there is also a certain amount of C or N in the system, more complex species such as C–H and N–H bonds will form at reduced conditions (Armstrong et al. 2015; Li et al. 2017). However, H species in bridgmanite and silicate melt at high pressures and varying oxygen fugacity conditions are still poorly constrained.

5 Conclusion

With a comprehensive review of studies regarding the solubility of water in bridgmanite, the conclusions of this article are summarized as follows:

1. The water solubility of bridgmanite obtained from both HPHT experiments and first-principles simulations is highly uncertain. Experimental results could range from ten to thousands of µg/g, while computational results could vary by three orders of magnitude. The significant uncertainty in water solubility of bridgmanite hinders its further applications on constraining water budgets in the lower mantle.
2. Innovative research protocol is urgently needed to address the huge controversy, especially the quantitative analysis techniques for determining the water content of tiny sample recovery from HTHP experiments.
3. Based on the previous point, extensive work is ahead to clarify the behavior of H dissolving in bridgmanite at varying P–T, oxygen fugacity, and composition conditions, to deepen our understanding of water in Earth's deep mantle.

Acknowledgements Y. Li appreciates the support of the National Science Fund for Distinguished Young Scholars (Grant No. 42225302).

Author contributions WL: Conceptualization, Data collection, Writing-original draft, Review & Editing. YL: Conceptualization, Supervision, Funding acquisition, Review & Editing.

Funding National Science Fund for Distinguished Young Scholars (Grant No. 42225302) to Yuan Li.

Data availability All data is available in the main text.

Declarations

Conflict of interest The authors declare that they have no known competing interests that could have appeared to influence this paper.

Ethical approval All authors have approved the manuscript and agree with its submission.

References

- Armstrong LS, Hirschmann MM, Stanley BD et al (2015) Speciation and solubility of reduced C–O–H–N volatiles in mafic melt: implications for volcanism, atmospheric evolution, and deep volatile cycles in the terrestrial planets. *Geochim Cosmochim Acta* 171:283–302. <https://doi.org/10.1016/j.gca.2015.07.007>
- Bercovici D, Karato S (2003) Whole-mantle convection and the transition-zone water filter. *Nature* 425:39–44. <https://doi.org/10.1038/nature01918>

- Boehler R (2000) High-pressure experiments and the phase diagram of lower mantle and core materials. *Rev Geophys* 38:221–245. <https://doi.org/10.1029/1998RG000053>
- Bolfan-Casanova N, Keppler H, Rubie DC (2000) Water partitioning between nominally anhydrous minerals in the $\text{MgO}-\text{SiO}_2-\text{H}_2\text{O}$ system up to 24 GPa: implications for the distribution of water in the Earth's mantle. *Earth Planet Sci Lett* 182:209–221. [https://doi.org/10.1016/S0012-821X\(00\)00244-2](https://doi.org/10.1016/S0012-821X(00)00244-2)
- Bolfan-Casanova N, Keppler H, Rubie DC (2003) Water partitioning at 660 km depth and evidence for very low water solubility in magnesium silicate perovskite. *Geophys Res Lett*. <https://doi.org/10.1029/2003GL017182>
- Boujibar A, Bolfan-Casanova N, Andrault D et al (2016) Incorporation of Fe^{2+} and Fe^{3+} in bridgmanite during magma ocean crystallization. *Am Mineral* 101:1560–1570. <https://doi.org/10.2138/am-2016-5561>
- Di Genova D, Bondar D, Zandonà A et al (2023) Viscosity of anhydrous and hydrous peridotite melts. *Chem Geol* 625:121440. <https://doi.org/10.1016/j.chemgeo.2023.121440>
- Dixon JE, Leist L, Langmuir C, Schilling J-G (2002) Recycled dehydrated lithosphere observed in plume-influenced mid-ocean-ridge basalt. *Nature* 420:385–389. <https://doi.org/10.1038/nature01215>
- Fei H, Katsura T (2020) High water solubility of ringwoodite at mantle transition zone temperature. *Earth Planet Sci Lett* 531:115987. <https://doi.org/10.1016/j.epsl.2019.115987>
- Fei H, Yamazaki D, Sakurai M et al (2017) A nearly water-saturated mantle transition zone inferred from mineral viscosity. *Sci Adv* 3:e1603024. <https://doi.org/10.1126/sciadv.1603024>
- Fiquet G, Auzende AL, Siebert J et al (2010) Melting of peridotite to 140 gigapascals. *Science* 329:1516–1518. <https://doi.org/10.1126/science.1192448>
- French SW, Romanowicz B (2015) Broad plumes rooted at the base of the Earth's mantle beneath major hotspots. *Nature* 525:95–99. <https://doi.org/10.1038/nature14876>
- Frost DJ, McCammon CA (2008) The redox state of Earth's mantle. *Annu Rev Earth Planet Sci* 36:389–420. <https://doi.org/10.1146/annurev.earth.36.031207.124322>
- Fu S, Yang J, Karato S et al (2019) Water concentration in single-crystal (Al,Fe)-bearing bridgmanite grown from the hydrous melt: implications for dehydration melting at the topmost lower mantle. *Geophys Res Lett* 46:10346–10357. <https://doi.org/10.1029/2019GL084630>
- Gaetani GA, Grove TL (1998) The influence of water on melting of mantle peridotite. *Contrib Miner Petrol* 131:323–346
- Gault B, Chiaramonti A, Cojocaru-Mirédin O et al (2021) Atom probe tomography. *Nat Rev Methods Prim* 1:1–30. <https://doi.org/10.1038/s43586-021-00047-w>
- Gu T, Pamato MG, Novella D et al (2022) Hydrous peridotitic fragments of Earth's mantle 660 km discontinuity sampled by a diamond. *Nat Geosci*. <https://doi.org/10.1038/s41561-022-01024-y>
- Hallis LJ, Huss GR, Nagashima K et al (2015) Evidence for primordial water in Earth's deep mantle. *Science* 350:795–797. <https://doi.org/10.1126/science.aac4834>
- Hernández ER, Alfè D, Brodholt J (2013) The incorporation of water into lower-mantle perovskites: a first-principles study. *Earth Planet Sci Lett* 364:37–43. <https://doi.org/10.1016/j.epsl.2013.01.005>
- Hirschmann MM (2006) Water, melting, and the deep Earth H_2O cycle. *Annu Rev Earth Planet Sci* 34:629–653. <https://doi.org/10.1146/annurev.earth.34.031405.125211>
- Hirschmann MM, Dasgupta R (2009) The H/C ratios of Earth's near-surface and deep reservoirs, and consequences for deep Earth volatile cycles. *Chem Geol* 262:4–16. <https://doi.org/10.1016/j.chemgeo.2009.02.008>
- Hirschmann MM, Withers AC, Ardia P, Foley NT (2012) Solubility of molecular hydrogen in silicate melts and consequences for volatile evolution of terrestrial planets. *Earth Planet Sci Lett* 345–348:38–48. <https://doi.org/10.1016/j.epsl.2012.06.031>
- Inoue T, Wada T, Sasaki R, Yurimoto H (2010) Water partitioning in the Earth's mantle. *Phys Earth Planet Inter* 183:245–251. <https://doi.org/10.1016/j.pepi.2010.08.003>
- Irfune T, Tsuchiya T (2015) Phase transitions and mineralogy of the lower mantle. *Treatise on geophysics*. Elsevier, pp 33–60
- Ishii T, Ohtani E, Shatskiy A (2022) Aluminum and hydrogen partitioning between bridgmanite and high-pressure hydrous phases: implications for water storage in the lower mantle. *Earth Planet Sci Lett* 583:117441. <https://doi.org/10.1016/j.epsl.2022.117441>
- Ito E, Weidner DJ (1986) Crystal growth of MgSiO_3 perovskite. *Geophys Res Lett* 13:464–466. <https://doi.org/10.1029/GL013i005p00464>
- Ito E, Kubo A, Katsura T, Walter MJ (2004) Melting experiments of mantle materials under lower mantle conditions with implications for magma ocean differentiation. *Phys Earth Planet Inter* 143–144:397–406. <https://doi.org/10.1016/j.pepi.2003.09.016>
- Karato S (2011) Water distribution across the mantle transition zone and its implications for global material circulation. *Earth Planet Sci Lett* 301:413–423. <https://doi.org/10.1016/j.epsl.2010.11.038>
- Karato S, Karki B, Park J (2020) Deep mantle melting, global water circulation and its implications for the stability of the ocean mass. *Prog Earth Planet Sci* 7:76. <https://doi.org/10.1186/s40645-020-00379-3>
- Keppler H, Bolfan-Casanova N (2006) Thermodynamics of water solubility and partitioning. *Rev Mineral Geochem* 62:193–230. <https://doi.org/10.2138/rmg.2006.62.9>
- Ko B, Greenberg E, Prakapenka V et al (2022) Calcium dissolution in bridgmanite in the Earth's deep mantle. *Nature* 611:88–92. <https://doi.org/10.1038/s41586-022-05237-4>
- Koga K, Hauri E, Hirschmann M, Bell D (2003) Hydrogen concentration analyses using SIMS and FTIR: comparison and calibration for nominally anhydrous minerals. *Geochem Geophys Geosyst*. <https://doi.org/10.1029/2002GC000378>
- Kuwahara H, Nakada R (2023) Partitioning of Fe_{2+} and Fe_{3+} between bridgmanite and silicate melt: implications for redox evolution of the Earth's mantle. *Earth Planet Sci Lett* 615:118197. <https://doi.org/10.1016/j.epsl.2023.118197>
- Li Y, Dasgupta R, Tsuno K (2017) Carbon contents in reduced basalts at graphite saturation: implications for the degassing of mars, mercury, and the moon: carbon in reduced planetary basalts. *J Geophys Res Planets* 122:1300–1320. <https://doi.org/10.1002/2017JE005289>
- Li Y, Vočadlo L, Sun T, Brodholt JP (2020) The Earth's core as a reservoir of water. *Nat Geosci* 13:453–458. <https://doi.org/10.1038/s41561-020-0578-1>
- Libowitzky E, Rossman GR (1997) An IR absorption calibration for water in minerals. *Am Mineral* 82:1111–1115. <https://doi.org/10.2138/am-1997-11-1208>
- Litasov K, Ohtani E, Langenhorst F et al (2003) Water solubility in Mg-perovskites and water storage capacity in the lower mantle. *Earth Planet Sci Lett* 211:189–203. [https://doi.org/10.1016/S0012-821X\(03\)00200-0](https://doi.org/10.1016/S0012-821X(03)00200-0)
- Liu Z, Park J, Karato S (2016) Seismological detection of low-velocity anomalies surrounding the mantle transition zone in Japan subduction zone. *Geophys Res Lett* 43:2480–2487. <https://doi.org/10.1002/2015GL067097>
- Liu J, Xia Q-K, Kuritani T et al (2017a) Mantle hydration and the role of water in the generation of large igneous provinces. *Nat Commun* 8:1824. <https://doi.org/10.1038/s41467-017-01940-3>
- Liu Z, Nishi M, Ishii T et al (2017b) Phase relations in the system $\text{MgSiO}_3-\text{Al}_2\text{O}_3$ up to 2300 K at lower mantle pressures.

- J Geophys Res Solid Earth 122:7775–7788. <https://doi.org/10.1002/2017JB014579>
- Liu Z, McCammon C, Wang B et al (2020) Stability and solubility of the FeAlO₃ component in bridgmanite at uppermost lower mantle conditions. J Geophys Res Solid Earth. <https://doi.org/10.1029/2019JB018447>
- Liu Z, Fei H, Chen L et al (2021) Bridgmanite is nearly dry at the top of the lower mantle. Earth Planet Sci Lett 570:117088. <https://doi.org/10.1016/j.epsl.2021.117088>
- Marty B (2012) The origins and concentrations of water, carbon, nitrogen and noble gases on Earth. Earth Planet Sci Lett 313–314:56–66. <https://doi.org/10.1016/j.epsl.2011.10.040>
- Meade C, Reffner JA, Ito E (1994) Synchrotron infrared absorbance measurements of hydrogen in MgSiO₃ perovskite. Science 264:1558–1560. <https://doi.org/10.1126/science.264.5165.1558>
- Moore JG (1970) Water content of basalt erupted on the ocean floor. Contr Mineral Petrol 28:272–279. <https://doi.org/10.1007/BF00388949>
- Murakami M, Hirose K, Yurimoto H et al (2002) Water in Earth's lower mantle. Science 295:1885–1887. <https://doi.org/10.1126/science.1065998>
- Murakami M, Hirose K, Kawamura K et al (2004) Post-perovskite phase transition in MgSiO₃. Science 304:855–858. <https://doi.org/10.1126/science.1095932>
- Navrotsky A (1999) A lesson from ceramics. Science 284:1788–1789. <https://doi.org/10.1126/science.284.5421.1788>
- Navrotsky A, Schoenitz M, Kojitani H et al (2003) Aluminum in magnesium silicate perovskite: formation, structure, and energetics of magnesium-rich defect solid solutions. J Geophys Res Solid Earth. <https://doi.org/10.1029/2002JB002055>
- Newcombe ME, Nielsen SG, Peterson LD et al (2023) Degassing of early-formed planetesimals restricted water delivery to Earth. Nature. <https://doi.org/10.1038/s41586-023-05721-5>
- Oganov AR, Ono S (2004) Theoretical and experimental evidence for a post-perovskite phase of MgSiO₃ in Earth's D'' layer. Nature 430:445–448. <https://doi.org/10.1038/nature02701>
- Ohtani E (2021) Hydration and dehydration in Earth's interior. Annu Rev Earth Planet Sci 49:253–278. <https://doi.org/10.1146/annurev-earth-080320-062509>
- Panero WR, Pigott JS, Reaman DM et al (2015) Dry (mg,Fe)SiO₃ perovskite in the Earth's lower mantle. J Geophys Res Solid Earth 120:894–908. <https://doi.org/10.1002/2014JB011397>
- Paterson M (1982) The determination of hydroxyl by infrared absorption in quartz, silicate glasses and similar materials. Bull de Minéralogie 105:20–29. <https://doi.org/10.3406/bulmi.1982.7582>
- Peslier AH, Schönbächler M, Busemann H, Karato S-I (2017) Water in the Earth's interior: distribution and origin. Space Sci Rev 212:743–810. <https://doi.org/10.1007/s11214-017-0387-z>
- Reddy SM, Saxe DW, Rickard WDA et al (2020) Atom probe tomography: development and application to the geosciences. Geostand Geoanal Res 44:5–50. <https://doi.org/10.1111/ggr.12313>
- Ross NL, Gibbs GV, Rosso KM (2003) Potential docking sites and positions of hydrogen in high-pressure silicates. Am Mineral 88:1452–1459. <https://doi.org/10.2138/am-2003-1009>
- Rossmann GR (2006) Analytical methods for measuring water in nominally anhydrous minerals. Rev Mineral Geochem 62:1–28. <https://doi.org/10.2138/rmg.2006.62.1>
- Saal AE, Hauri EH, Cascio ML et al (2008) Volatile content of lunar volcanic glasses and the presence of water in the moon's interior. Nature 454:192–195. <https://doi.org/10.1038/nature07047>
- Schmandt B, Jacobsen SD, Becker TW et al (2014) Dehydration melting at the top of the lower mantle. Science 344:1265–1268. <https://doi.org/10.1126/science.1253358>
- Stixrude L (2001) First principles theory of mantle and core phases. Rev Mineral Geochem 42:319–343. <https://doi.org/10.2138/rmg.2001.42.9>
- Townsend JP, Tsuchiya J, Bina CR, Jacobsen SD (2015) First-principles investigation of hydrous post-perovskite. Phys Earth Planet Inter 244:42–48. <https://doi.org/10.1016/j.pepi.2015.03.010>
- Townsend JP, Tsuchiya J, Bina CR, Jacobsen SD (2016) Water partitioning between bridgmanite and postperovskite in the lowermost mantle. Earth Planet Sci Lett 454:20–27. <https://doi.org/10.1016/j.epsl.2016.08.009>
- Tschauner O, Ma C, Beckett JR et al (2014) Discovery of bridgmanite, the most abundant mineral in Earth, in a shocked meteorite. Science 346:1100–1102. <https://doi.org/10.1126/science.1259369>
- Yang X, Keppler H, Li Y (2016) Molecular hydrogen in mantle minerals. Geochim Persp Let. <https://doi.org/10.7185/geochemlet.1616>
- Yang Y-N, Du Z, Lu W et al (2023) NanoSIMS analysis of water content in bridgmanite at the micron scale: an experimental approach to probe water in Earth's deep mantle. Front Chem 11:1166593
- Zhang H, Egbert GD, Huang Q (2022) A relatively dry mantle transition zone revealed by geomagnetic diurnal variations. Sci Adv 8:eab03293. <https://doi.org/10.1126/sciadv.ab03293>

Springer Nature or its licensor (e.g. a society or other partner) holds exclusive rights to this article under a publishing agreement with the author(s) or other rightsholder(s); author self-archiving of the accepted manuscript version of this article is solely governed by the terms of such publishing agreement and applicable law.